Journal of Applied Sciences

ISSN 1812-5654

science alert

ANSInet
an open access publisher
http://ansinet.com

Journal of Applied Sciences 6 (6): 1351-1361, 2006
ISSN 1812-5654

Boundary Mapping of Chromosome Spread Images Using Optimal Set of Parameter Values in Discrete Cosine Transform Based Gradient Vector Flow Active Contours

[1]A. Prabhu Britto and [2]G. Ravindran
[1]Center for Medical Electronics, Department of Electronics and Communication Engineering,
[2]Faculty of Information and Communication Engineering, Anna University, Chennai 600025, India

Abstract: This study proposed to identify and investigate optimality of Discrete Cosine Transform (DCT) based Gradient Vector Flow (GVF) active contours and this research is expected to yield a robust technique which can be used to boundary map chromosome images having variability in shape and size, from chromosome spread images. Weak edges are also manifested here. GVF field active contours are found to have good convergence properties. The energy compaction is enhanced by incorporating the DCT into the segmentation scheme. A unique set of parameter values for the technique is required for boundary mapping every chromosome image. Characterization studies have shown that an optimal range of values exists for each parameter within which good boundary mapping results can be obtained for various chromosomes in similar class of images.

Key words: Gradient vector flow, active contours, discrete cosine transform, chromosome, boundary mapping, characterization

INTRODUCTION

Discrete Cosine Transform (DCT) based Gradient Vector Flow (GVF) active contours are used to obtain accurate segmentation results from a class of chromosome images that have variable properties in shape, size and other image properties. Boundary mapping is a segmentation approach that can be done easily in noise-free high contrast images by employing low-level techniques, traditional edge detectors, region growing or mathematical morphology. Noise and artifacts can possibly cause incorrect segmentation or boundary discontinuities in segmented objects (Mclnerney and Terzopoulous, 1996). The classical boundary mapping techniques, namely, region growing, relaxation labeling, edge detection and linking suffer from limitations leading to incorrect assumptions during the boundary integration process.

ACTIVE CONTOUR MODELS

Active contours also called as snakes or deformable curves, first proposed by Kass *et al.* (1987) are energy-minimizing contours that apply information about the boundaries as part of an optimization procedure. They are generally initialized around the object of interest by automatic or manual process. The contour then deforms itself from its initial position in conformity with nearest dominant edge feature by minimizing the energy composed of the internal and external forces. The energy is composed of the internal and external forces. Internal forces which enforce smoothness of the curve are computed from within the active contour. External forces derived from the image help to drive the curve toward the desired features of interest during the course of the iterative process. The energy function is minimized, thus making the model active.

The energy minimization process can be viewed as a dynamic problem where the active contour model is governed by the laws of elasticity and lagrangian dynamics (Rueckert, 1997) and the model evolves until equilibrium of all forces is reached, which is equivalent to a minimum of the energy function.

FORMULATION OF ACTIVE CONTOUR MODELS

An active contour model can be represented by a curve c, as a function of its arc length τ,

$$c(\tau) = \begin{pmatrix} x(\tau) \\ y(\tau) \end{pmatrix} \quad (1)$$

with $\tau = [0...1]$.

Corresponding Author: A. Prabhu Britto, Center for Medical Electronics,
Department of Electronics and Communication Engineering, Anna University, Chennai 600025, India

To define a closed curve c(0) is set to equal c(1). A discrete model can be expressed as an ordered set of n vertices $v_i = (x_i,y_i)^T$ with $v=(v_1,\ldots,v_n)$. The large number of vertices required to achieve accuracy could lead to high computational complexity and numerical instability (Rueckert, 1997). Mathematically, an active contour model can be defined in discrete form as a curve x(s)= [x(s), y(s)], sε[1,0] that moves through the spatial domain of an image to minimize the energy functional:

$$E = \int_0^1 \frac{1}{2}(\alpha|x'(s)|^2 + \beta|x''(s)|^2 + E_{est}(x(s))ds \quad (2)$$

Where, α and β are weighting parameters that control the active contour's tension and rigidity, respectively (Xu and Prince, 1997). The first order derivative discourages stretching and the second order derivative discourages bending. The weighting parameters of tension and rigidity, viz., α and β govern the effect of the derivatives on the snake. The external energy function E_{ext} is derived from the image so that it takes on its smaller values at the features of interest such as boundaries and guides the active contour towards the boundaries. The external energy is defined by:

$$E_{ext} = \kappa|G_\sigma(x,y) * I(x,y)| \quad (3)$$

Where, $G_\sigma(x,y)$ is a two-dimensional Gaussian function with standard deviation σ, I(x,y) represents the image and κ is the external force weight. This external energy is specified for a line drawing (black on white) and positive κ is used. A motivation for applying some Gaussian filtering to the underlying image is to reduce noise.

An active contour that minimizes E must satisfy the Euler Equation

$$\alpha x''(s)-\beta x''''(s)-\nabla E_{ext}=0 \quad (4)$$

Where, $F_{int} = \alpha x''(s) - \beta x''''(s)$ and $F_{ext} = -\nabla E_{ext}$ comprise the components of a force balance equation such that:

$$F_{int} + F_{ext} = 0 \quad (5)$$

The internal force F_{int} discourages stretching and bending while the external potential force F_{ext} drives the active contour towards the desired image boundary. Equation 4 is solved by making the active contour dynamic by treating x as a function of time t as well as s. Then the partial derivative of x with respect to t is then set equal to the left hand side of Eq. 4 as follows:

$$x_t(s,t) = \alpha x''(s,t)-\beta x''''(s,t)-\nabla E_{ext} \quad (6)$$

A solution to Eq. 6 can be obtained by discretizing the equation and solving the discrete system iteratively (Kass *et al*., 1987). When the solution x(s,t) stabilizes, the term $x_t(s,t)$ vanishes and a solution of Eq. 4 is achieved.

Traditional active contour models suffer from a few drawbacks. Boundary concavities leave the contour split across the boundary. Capture range is also limited. Methods suggested to overcome these difficulties, namely multiresolution methods (Leroy *et al*., 1996), pressure forces (Cohen, 1991), distance potentials (Cohen and Cohen, 1993), control points (Davatzikos and Prince, 1994), domain adaptivity (Davatzikos and Prince, 1995), directional attractions (Abrantes and Marques, 1996) and solenoidal fields (Prince and Xu, 1996), however solved one problem but introduced new ones (Xu and Prince, 2000). Hence, a new class of external fields called GVF fields (Xu and Prince, 2000; 1998) was suggested to overcome the difficulties in traditional active contour models.

GRADIENT VECTOR FLOW (GVF) ACTIVE CONTOURS

GVF active contours use GVF fields obtained by solving a vector diffusion equation that diffuses the gradient vectors of a gray-level edge map computed from the image. The GVF active contour model cannot be written as the negative gradient of a potential function. Hence it is directly specified from a dynamic force equation, instead of the standard energy minimization network.

The external forces arising out of GVF fields are non-conservative forces as they cannot be written as gradients of scalar potential functions. The usage of non-conservative forces as external forces show improved performance of GVF field active contours compared to traditional energy-minimizing active contours (Xu and Prince, 2000; 1998).

The GVF field points towards the object boundary when very near to the boundary, but varies smoothly over homogeneous image regions extending to the image border. Hence the GVF field can capture an active contour from long range from either side of the object boundary and can force it into the object boundary. The gradient vectors are normal to the boundary surface but by combining Laplacian and Gradient the result is not the normal vectors to the boundary surface. As a result of this, the GVF field yields vectors that point into boundary concavities so that the active contour is driven through the concavities. Hence, the GVF active contour model is insensitive to the initialization of the contour and it is able to move into boundary concavities.

Information regarding whether the initial contour should expand or contract need not be given to the GVF active contour model. The GVF active contour model has

a large capture range. The GVF is very useful when there are boundary gaps, because it preserves the perceptual edge property of active contours (Kass *et al*., 1987; Xu and Prince, 1998). Also, the GVF provides for flexible initialization of the initial contour.

The GVF field is defined as the equilibrium solution (Xu and Prince, 2000) to the following vector diffusion equation:

$$u_t = g(|\nabla f|)\nabla^2 u - h(|\nabla f|)(u-\nabla f) \quad (7a)$$

$$u(x,0) = \nabla f(x) \quad (7b)$$

Where, u_t denotes the partial derivative of u(x,t) with respect to t, ∇^2 is the Laplacian operator (applied to each spatial component of u separately) and f is an edge map that has a higher value at the desired object boundary. The functions in "g" and "h" control the amount of diffusion in GVF. In Eq. 7, $g(|\nabla f|)\nabla^2 u$ produces a smoothly varying vector field and hence called as the smoothing term, while $h(|\nabla f|)(u-\nabla f)$ encourages the vector field u to be close to ∇f computed from the image data and hence called as the data term. The weighting functions g(•) and h(•) apply to the smoothing and data terms respectively and they are chosen as Xu and Prince (1998) $g(|\nabla f|)=\mu$ and $h(|\nabla f|)=|\nabla f|^2$. g(•) is constant here and smoothing occurs everywhere, while h(•) grows larger near strong edges and dominates at boundaries. Hence, the Gradient Vector Flow field is defined as the vector field v(x,y)=[u(x,y),v(x,y)] that minimizes the energy functional:

$$\varepsilon = \int\int \mu(u_x^2 + u_y^2 + v_x^2 + v_y^2) + |\nabla f|^2 |v - \nabla f|^2 dxdy \quad (8)$$

The effect of this variational formulation is that the result is made smooth when there is no data.

When the gradient of the edge map is large, it keeps the external field nearly equal to the gradient, but keeps field to be slowly varying in homogeneous regions where the gradient of the edge map is small, i.e., the gradient of an edge map ∇f has vectors point toward the edges, which are normal to the edges at the edges and have magnitudes only in the immediate vicinity of the edges and in homogeneous regions ∇f is nearly zero. μ is a regularization parameter that governs the tradeoff between the first and the second term in the integrand in Eq. 8. The solution of Eq. 8 can be done using the Calculus of Variations and further by treating u and v as functions of time, solving them as generalized diffusion equations (Xu and Prince, 1998).

DISCRETE COSINE TRANSFORM (DCT) BASED GVF ACTIVE CONTOURS

Transform theory plays a fundamental role in image processing. The transform of an image yields more insight into the properties of the image. The various image transforms that are in use are the fast fourier transform, walsh transform, hadamard transform, haar transform, slant transform and the DCT . DCcan be computed via fast algorithms like the FFT and it has excellent energy compaction. Hence, the Discrete Cosine Transform promises better description of the image properties. Therefore the DCT is embedded into the boundary mapping scheme to obtain better energy compaction. The 2D DCT is defined as:

$$C(u,v) = \alpha(u)\alpha(v)\sum_{x=0}^{N-1}\sum_{y=0}^{N-1} f(x,y)\cos\left[\frac{(2x+1)u\pi}{2N}\right]\cos\left[\frac{(2y+1)v\pi}{2N}\right] \quad (9)$$

The local contrast of the Image at the given pixel location (k,l) is given by:

$$P(k,l) = \frac{\sum_{t=1}^{2(2n+1)-1} w_t E_t}{d_{00}} \quad (10)$$

where,

$$E_t = \frac{\sum_{u+v=t} |d_{u,v}|}{N} \quad (11)$$

and

$$N = \begin{cases} t+1 & t<2n+1 \\ 2(2n+1)-t & t\geq 2n+1 \end{cases} \quad (12)$$

Here, w_t denotes the weights used to select the DCT coefficients. The local contrast P(k,l) is then used to generate a DCT contrast enhanced image (Tang and Acton, 2004), which is then subject to selective segmentation by the energy compact gradient vector flow active contour model using Eq. 8.

RESULTS AND DISCUSSION

The chromosome metaphase image shown in Fig. 1 having size 480x512 pixels at 72 pixels per inch resolution was provided by Prof. Ken Castleman and Prof. Qiang Wu, from Advanced Digital Imaging Research, Texas.

Fig. 1: Original chromosome spread image (Courtesy: Prof. Ken Castleman and Prof. Qiang Wu, advanced digital imaging research, texas)

Insignificant and unnecessary regions in the image were removed interactively. The chromosome of interest was selected from the chromosome spread image by user selection of a few points that formed the vertices of a polygon. On constructing the perimeter of the polygon from the selection points, seed points for the initial contour were automatically determined by periodically selecting every third pixel along the perimeter of the polygon. The GVF deformable curve was then allowed to deform until it converged to the chromosome boundary. The optimum parameters for the deformable curve with respect to the Chromosome images were determined by tabulated studies. The image was made to undergo minimal preprocessing so that the goal of boundary mapping in chromosome images with very weak edges is maintained.

The DCT based GVF Active contour is governed by the following parameters, namely, σ, μ, α, β and κ. σ determines the Gaussian filtering that is applied to the image to generate the external field. Larger value of σ will cause the boundaries to become blurry and distorted and can also cause a shift in the boundary location. However, large values of σ are necessary to increase the capture range of the active contour.

Micro is a regularization parameter in Eq. 8 and requires a higher value in the presence of noise in the image. α determines the tension of the active contour and β determines the rigidity of the contour. The tension keeps the active contour contracted and the rigidity keeps it smooth. α and β may also take on value zero implying that the influence of the respective tension and rigidity terms in the diffusion equation is low. κ is the external force weight that determines the strength of the external field that is applied. The iterations were set suitably.

Experimental results: Chromosome spread image samples, their corresponding DCT based GVF vector fields and their output images are presented in Fig. 2-13.

The output images indicate successful boundary mapping of chromosome images using DCT based GVF Active Contours (Fig. 2-13).

Experimental validation: In order to quantify the performance of a segmentation method, validation experiments are necessary. Validation is typically performed using one of two different types of truth models. In this study, ground truth model is not available and hence validation is performed on ordinal or ranking scale and then quantified. For experimental validation, a set of 10 random samples is taken and characterization of each parameter is done. The outputs were tabulated in ranking order with "1" describing the best quality output and as the quality decreases the rank increases up to rank 97. Rank 98 is a special case, where the output image is rejected based on quality or the output image is not available due to numerical instability possibly caused due to the greater number of contour points (Rueckert, 1997). The tables represent characterization studies for each parameter. Each table denotes variation for only one parameter either between the lower and upper limits of the parameter or between the lower and upper limits giving significantly different output, with the other parameters taking a constant value. The best parameter value of that table is the one that gives maximum good quality outputs for all samples or a majority of samples, as the study is done exhaustively on every parameter treating the other parameters as constants.

The statistical median is used to judge the distribution of values for each parameter value for all samples. When the median leans towards the lower values, i.e., towards "1", it indicates that almost 50% of the outputs lean towards "1", making that particular parameter value an optimal one and that optimal value is chosen. The characterization studies reveal that each parameter sometimes has an optimal range within which it can assume any value thereby giving majority good outputs for all samples. But for the sake of experimental purposes, only that investigated discrete value of each parameter that gave best output was chosen.

An important point to be noted is that characterization studies have been performed for those parameter values which give either significant output or significant difference in performance between adjacent parameter values. Those parameter values where there is no significant difference between adjacent parameter values have not been tabulated. Also, those parameter values outside the tabulated range which gave no proper results have not been tabulated.

Hence the optimal set of parameter values that give good boundary mapping for the given class of chromosome images is $\sigma = 0.25$, $\mu = 0.075$, $\alpha = 0$, $\beta = 0$ and $\kappa = 0.625$. A safe limit of 5% tolerance can be introduced to the optimal range of parameter values to make them suitable for use in similar classes of chromosome spread images as indicated in Table 6.

Statistical validation: The parameters act independently on the boundary mapping scheme. In each characterization, the effect of other parameters will also be felt as they assume a definite constant value. In the course of the characterization study from Table 1 to 5, optimum values for the respective parameters are chosen and applied as constant in the characterization study of the next parameter in the successive table. In the last

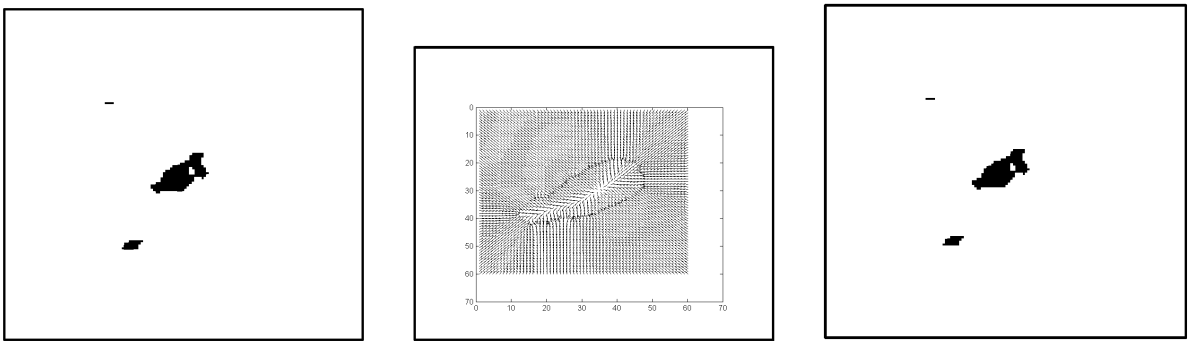

(a) (b) (c)

Fig. 2: a) The original image of Sample 2, b) corresponding DCT based GVF field, c) boundary mapped output image of Sample 2. The mapped boundary is indicated in red color

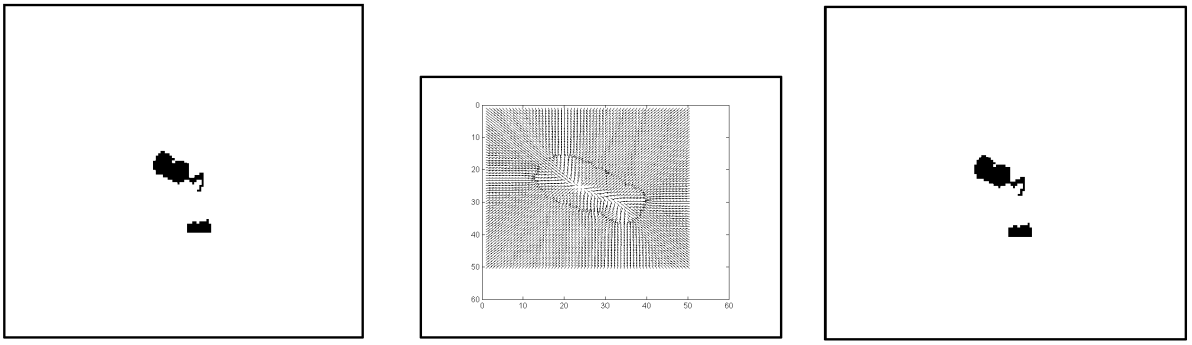

(a) (b) (c)

Fig. 3: a) The original image of Sample 3, b) corresponding DCT based GVF field, c) boundary mapped output image of Sample 3. The mapped boundary is indicated in red color

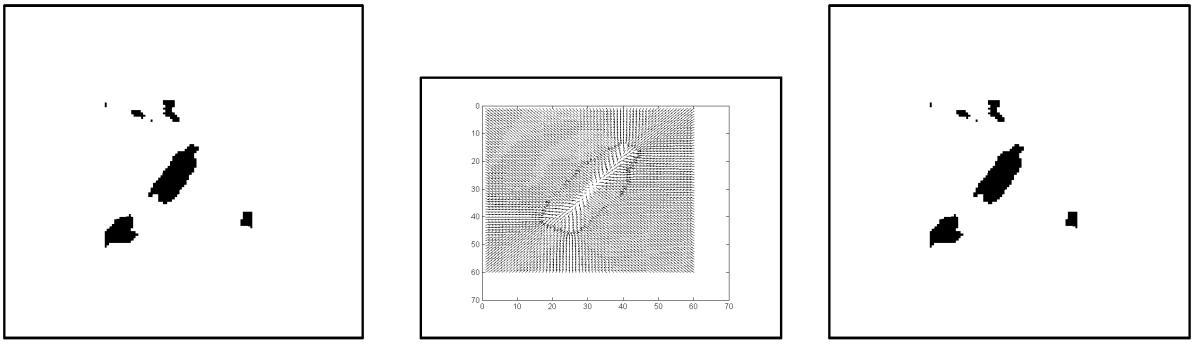

(a) (b) (c)

Fig. 4: a) The original image of Sample 4, b) corresponding DCT based GVF field, c) boundary mapped output image of Sample 4. The mapped boundary is indicated in red color

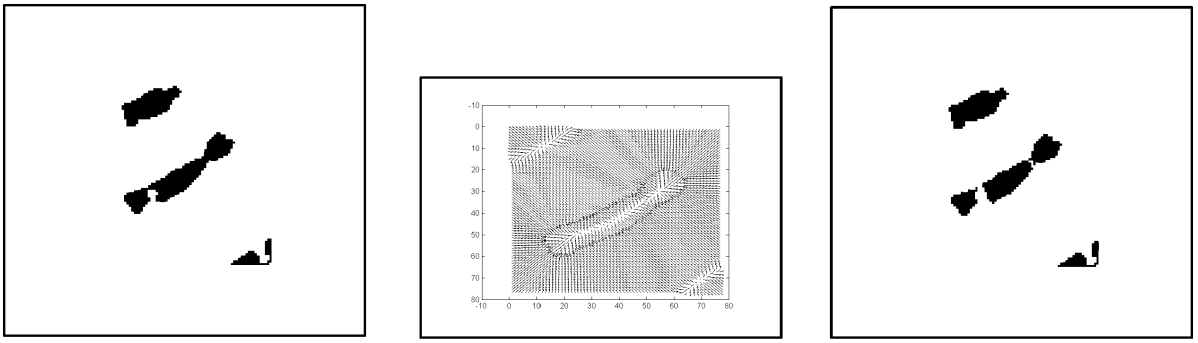

(a) (b) (c)

Fig. 5: a) The original image of Sample 5, b) corresponding DCT based GVF field, c) boundary mapped output image of Sample 5. The mapped boundary is indicated in red color

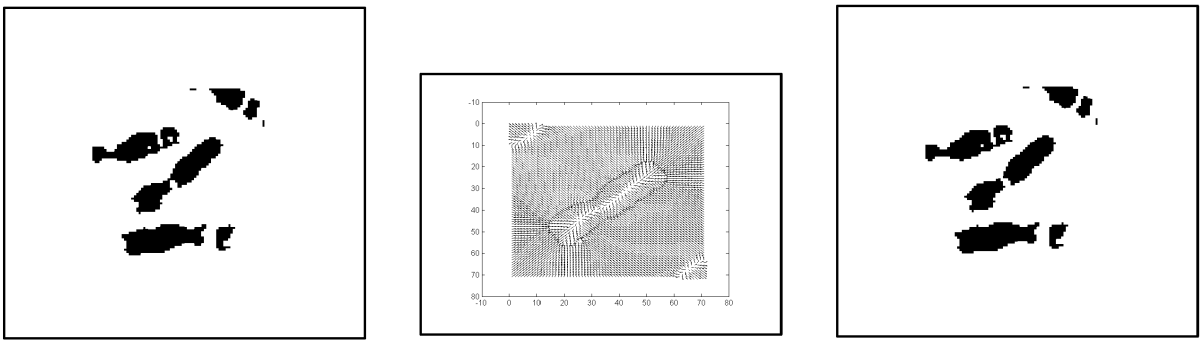

(a) (b) (c)

Fig. 6: a) The original image of Sample, b) corresponding DCT based GVF field, c) boundary mapped output image of Sample 6. The mapped boundary is indicated in red color

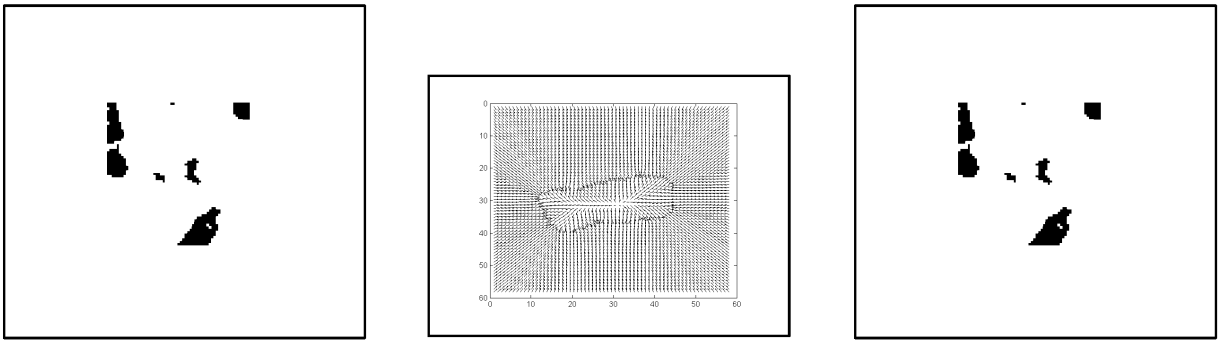

(a) (b) (c)

Fig. 7: a) The original image of Sample 7, b) corresponding DCT based GVF field, c) boundary mapped output image of Sample 7. The mapped boundary is indicated in red color

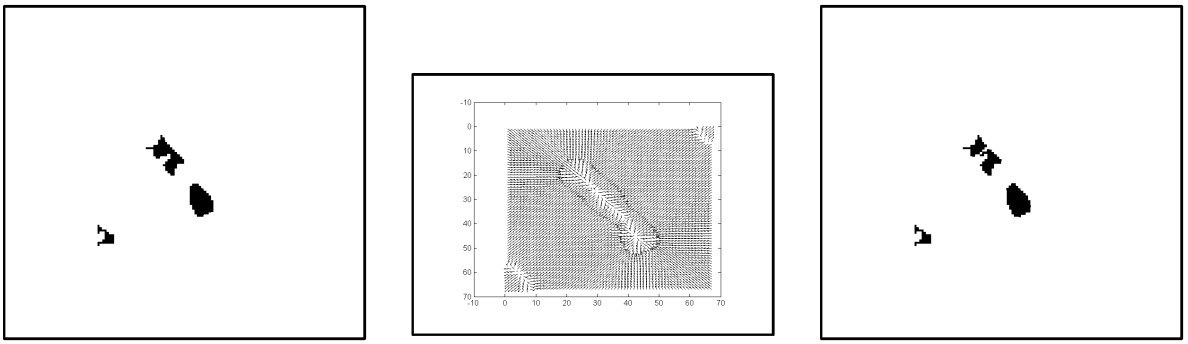

(a) (b) (c)

Fig. 8: a) The original image of Sample 8, b) corresponding DCT based GVF field, c) boundary mapped output image of Sample 8. The mapped boundary is indicated in red color

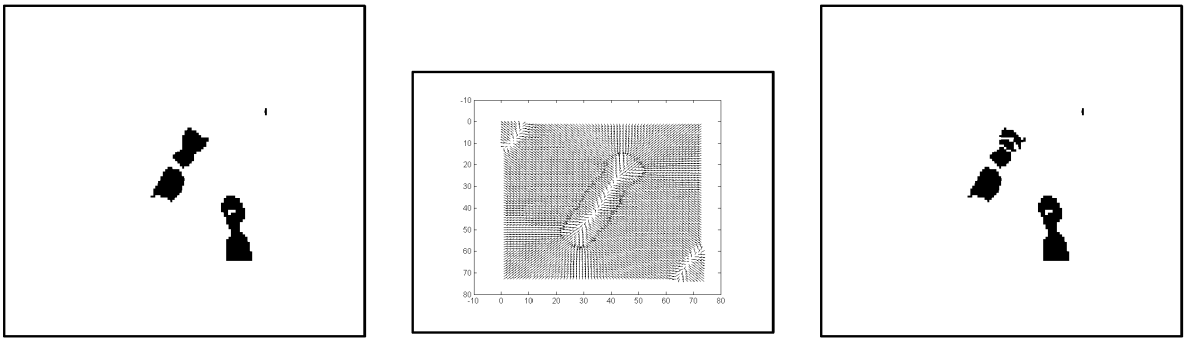

(a) (b) (c)

Fig. 9: a) The original image of Sample 9, b) corresponding DCT based GVF field, c) boundary mapped output image of Sample 9. The mapped boundary is indicated in red color

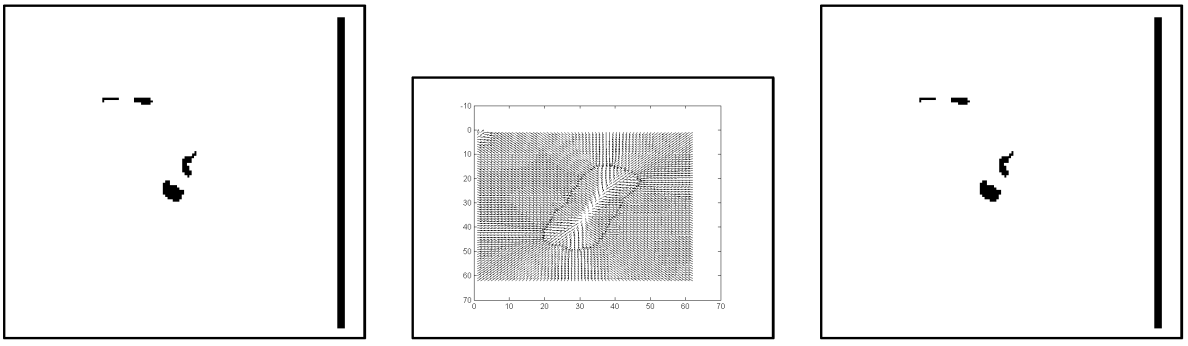

(a) (b) (c)

Fig. 10: a) The original image of Sample 10, b) corresponding DCT based GVF field, c) boundary mapped output image of Sample 10. The mapped boundary is indicated in red color

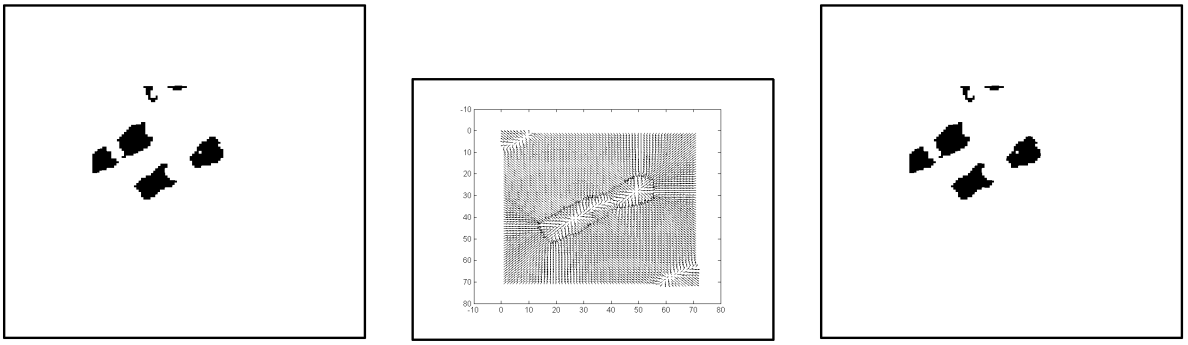

(a) (b) (c)

Fig. 11: a) The original image of Sample 11, b) corresponding DCT based GVF field, c) boundary mapped output image of Sample 11. The mapped boundary is indicated in red color

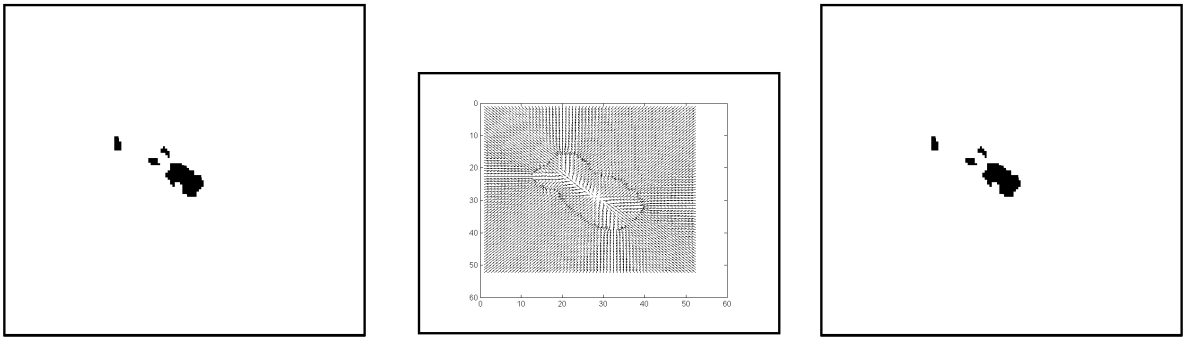

(a) (b) (c)

Fig. 12: a) The original image of Sample 12, b) corresponding DCT based GVF field, c) boundary mapped output image of Sample 12. The mapped boundary is indicated in red color

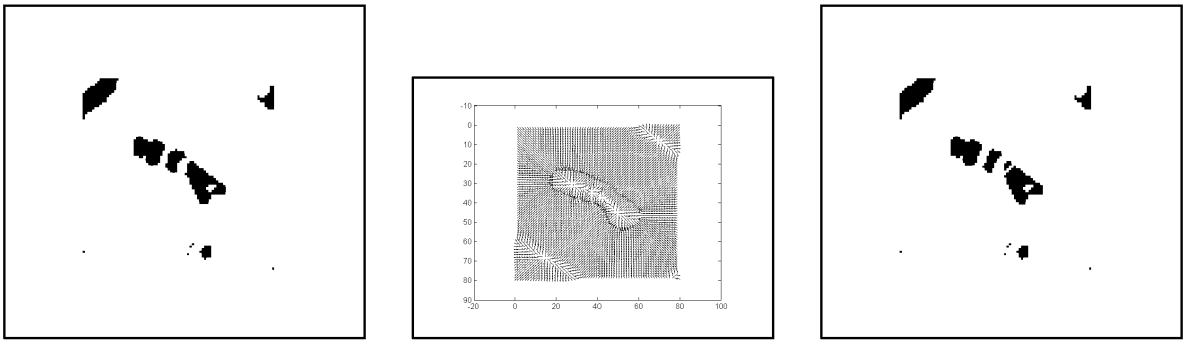

(a) (b) (c)

Fig. 13: a) The original image of Sample 13, b) corresponding DCT based GVF field, c) boundary mapped output image of Sample 13. The mapped boundary is indicated in red color

Table 1: Characterization of sigma

Sample	GVF (DCT) σ									
No.	0.05	0.1	0.15	0.2	0.25	0.5	0.6	0.8	1.0	1.2
1	77	77	77	77	77	29	77	29	13	77
2	77	77	77	29	13	13	13	13	29	77
3	97	77	34	29	77	29	78	81	75	78
4	77	77	29	29	31	70	79	79	79	78
5	97	97	97	97	98	98	98	98	98	98
6	86	86	46	38	38	14	38	38	46	78
7	97	97	97	97	98	98	98	98	98	98
8	86	86	86	54	98	98	98	98	98	98
9	77	77	77	77	38	46	15	77	13	79
10	86	77	13	77	46	65	78	13	78	77
Median	86	77	77	66	62	55	78	78	77	78

The median indicates that the acceptable optimal range of σ is 0.2 to 0.5. The best value compared qualitatively amongst those tested is 0.25 and hence it is chosen for performing further characterization.

Table 2: Characterization of Mu

Sample	GVF (DCT) μ					
No.	0.05	0.075	0.09375	0.1125	0.15	0.3
1	23	21	21	23	23	97
2	21	5	23	23	23	97
3	30	29	29	46	50	97
4	23	23	23	40	23	97
5	98	98	98	97	97	97
6	48	40	48	48	46	97
7	98	98	50	50	34	97
8	98	89	62	97	97	97
9	71	86	30	71	71	97
10	23	21	29	71	23	97
Median	39	35	29	49	40	97

The median indicates that the acceptable optimal range of μ is 0.05 to 0.09375. The best value compared qualitatively amongst those tested is 0.075 and hence it is chosen for performing further characterization.

Table 3: Characterization of alpha

Sample	GVF (DCT) α				
No.	0	0.125	0.25	0.5	1.0
1	7	23	77	71	77
2	7	30	29	77	30
3	5	67	78	78	67
4	23	23	79	80	80
5	98	98	98	98	97
6	98	48	40	46	87
7	98	98	98	97	97
8	90	86	62	97	94
9	21	23	23	71	27
10	5	7	23	21	71
Median	22	39	70	78	79

The median indicates that the acceptable optimal range of α extends from 0 to 0.125. The best value compared qualitatively amongst those tested is 0 and hence it is chosen for performing further characterization.

characterization study shown in Table 5, the values of σ, μ, α and β take on the chosen optimal values and only κ is investigated, thereby yielding a one way variation. Hence, one way analysis of variance on Table 5 is sufficient to test the significance of the entire boundary mapping process. A significant outcome from Table 5 will justify that the experimental results of Table 5 are valid, implying that the selected parameter values from Table 1 to 4 used as constants in Table 5 are also valid. Hence

Table 4: Characterization of beta

Sample	GVF (DCT) β		
No.	0.0	0.5	1.0
1	23	30	71
2	5	21	21
3	5	21	31
4	21	23	71
5	98	98	98
6	98	46	70
7	98	98	98
8	38	94	13
9	23	71	71
10	3	21	30
Median	23	38	71

The median indicates that the acceptable optimal range of β extends from 0 to 0.5. The best value compared qualitatively amongst those tested is 0 and hence it is chosen for performing further characterization.

Table 5: Characterization of kappa

Sample	GVF (DCT) κ					
No.	0	0.5	0.625	0.75	0.875	1.000
1	97	7	5	5	5	5
2	97	3	3	3	1	1
3	97	21	19	21	30	67
4	97	7	7	7	23	71
5	97	98	98	98	98	98
6	97	98	98	98	86	98
7	97	98	98	98	98	98
8	97	86	98	97	98	82
9	97	7	7	23	23	21
10	97	21	5	19	19	21
median	97	21	13	22	26	69

The median indicates that the acceptable optimal range of κ extends from 0.5 to 0.875. The best value compared qualitatively amongst those tested is 0.625.

Table 6: Optimal range of DCT based GVF active contour parameter values for chromosome spread images

Parameter GVC (DCT)	Chosen parameter value for tested spread image	Acceptable range of parameter values	Optimal range of values at 5% tolerance
σ	0.250	[0.20, 0.5]	[0.1900, 0.5250]
μ	0.075	[0.05, 0.09375]	[0.0475, 0.0984]
α	0.000	[0.00, 0.125]	[0.0000, 0.1313]
β	0.000	[0.00, 0.5]	[0.0000, 0.5250]
κ	0.625	[0.50, 0.875]	[0.4750, 0.9187]

The optimal range of parameter values is calculated from the acceptable range of parameter values by introducing a 5% tolerance to the lower and upper limits.

one way Anova test is performed on the last characterization (Table 5) to judge the experimental results. At the customary .05 significance level, one way Anova test yields a p value of 7.17082E-08 on Table 5, which rejects the null hypothesis. The very small p-value of 7.17082E-08 indicates that differences between the column means are highly significant. The probability of this outcome under the null hypothesis is less than 8 in 100,000,000. The test therefore strongly supports the alternate hypothesis that one or more of the samples are drawn from populations with different means. This implies that the results in Table 5 do not arise out of mere fluctuations and the results are actually significant.

Table 7: Calculated error measures for the 12 samples

Sample No.	Original image major axis length (pixels)	Contour image major axis length (pixels)	Error in maxor major axis length (pixels)	Original image minor axis length (pixels)	Contour image minor axis length (pixels)	Error in minor minor axis length (pixels)
1	39.673068	41.229220	1.556152	15.309357	16.309208	0.999851
2	31.063703	31.776621	0.712918	14.696620	15.662865	0.966245
3	38.900907	40.212541	1.311634	15.497664	16.359518	0.861854
4	70.118650	71.032654	0.914004	17.241634	18.791087	1.549452
5	57.781579	58.302327	0.520748	15.471960	16.374778	0.902819
6	36.164279	37.384992	1.220712	14.941666	15.585226	0.643560
7	52.453700	52.363700	-0.090000	13.251430	14.094662	0.843232
8	52.066324	52.978411	0.912087	15.394485	16.263917	0.869432
9	41.050011	42.358409	1.308398	17.451655	19.020988	1.569333
10	54.495901	54.316297	-0.179604	13.678191	14.134171	0.455980
11	31.806652	31.691938	-0.114715	15.565916	16.285951	0.720035
12	54.871574	54.551044	-0.320530	16.631023	17.047393	0.416370
Mean Diametric Error			0.645983667			0.899846917
Mean Radial Error			0.322991833			0.449923458

The very low values of the Radial Error in the detected boundary of the chromosome images (at 72 pixel per inch resolution) justify the efficiency and accuracy of the segmentation scheme.

Therefore the experimental results are valid. This justifies that a suitable value of parameter κ can be chosen from Table 5 and that the constant values of parameters σ, μ, α and β used in Table 5 are also valid as these values also have significant influence on the results tabulated in Table 5. Therefore, the experimental results and the inferences that are discussed in the previous paragraphs are also significant.

Error quantification: Any segmentation scheme has to be quantified in terms of the error, to justify its efficiency. Tabulation of the error in segmentation for the 12 samples (shown under subheading Experimental Results) is done. The error is calculated as a difference between the diametric lengths along the major and minor axis of the original image and the boundary mapped image correspondingly. Actual error measure is determined radially, which is half of the value of the diametric error. The mean error is calculated from the tabulated error values in Table 7.

CONCLUSIONS

The DCT based GVF Active Contours are well suited to the task of boundary mapping in chromosome spread images with the same optimal value of parameters for a class of images. This can be extended to other classes of chromosome spread images.

ACKNOWLEDGMENTS

The authors wish to thank Prof. Ken Castleman and Prof. Qiang Wu, both from Advanced Digital Imaging Research, Texas for their help in providing chromosome images.

REFERENCES

Abrantes, A.J. and J.S. Marques, 1996. A class of constrained clustering algorithms for object boundary extraction. IEEE Trans. on Image Processing, 5: 1507-1521.

Cohen, L.D., 1991. On active contours and balloons, CVGIP. Image Understanding, 53: 211-218.

Cohen, L.D. and I. Cohen, 1993. Finite-element methods for active contour models and balloons for 2-D and 3-D images, IEEE Trans. on Pattern Anal. Machine Intell., 15: 1131-1147.

Davatzikos, C. and J.L. Prince, 1994. Convexity analysis of active contour models. In: Proc. Conf. on Info. Sci. Sys., pp: 581-587.

Davatzikos, C. and J.L. Prince, 1995. An active contour model for mapping the cortex. IEEE Trans. on Medical Imaging, 14: 65-80.

Kass, M., A. Witkin and D. Terzopoulos, 1987. Snakes: Active contour models. Intl. J. Comp. Vision, 1: 321-331.

Leroy, B., I. Herlin and L.D. Cohen, 1996. Multi-resolution algorithms for active contour models. In 12th Intl. Conf. on Analysis and Optimization of Systems, pp: 58-65.

McInerney, T. and D. Terzopoulos, 1996. Deformable models in medical image analysis, IEEE Proc. Workshop Math. Methods in Biomedical Image Analysis, pp: 171-180.

Prince, J.L. and C. Xu, 1996. A new external force model for snakes. In: 1996 Image and Multidimensional Signal Processing Workshop, pp: 30-31.

Rueckert, D., 1997. Segmentation and Tracking in cardiovascular MR images using geometrically deformable models and templates. Ph.D. Thesis, Imperial College of Science, Technology and Medicine, London.

Tang, Jinshan and S.T. Acton, 2004. A DCT based gradient vector flow snake for object boundary detection. Image Analysis and Interpretation. 6th IEEE Southwest Symposium, pp: 157-161.

Xu, C. and J.L. Prince, 1997. Gradient Vector Flow: A New External Force for Snakes, IEEE Proc. Conf. Comp. Vis. Patt. Recog. (CVPR'97), pp: 66-71.

Xu, C. and J.L. Prince, 1998. Snakes, shapes and gradient vector flow. IEEE Trans. Image Processing, 7: 359-369.

Xu, C. and J.L. Prince, 2000. Gradient Vector Flow Deformable Models. In: Handbook of Medical Imaging, Academic Press, pp: 159-169.